

## UNDERSTANDING MODE TRANSITIONS IN VORTEX-INDUCED VIBRATION USING CONTROLLED MOTION

T. L. Morse & C. H. K. Williamson  
*Sibley School of Mechanical & Aerospace Engineering  
Cornell University, Ithaca, NY 14853, USA*

### ABSTRACT

*In this study we have made extensive measurements of the fluid forces on a cylinder that is controlled to oscillate transverse to a free stream at  $Re = 4000$ . These measurements were used to create extremely high resolution contour plots of the magnitude of the fluid force, and contour plots of the phase angle between the forces and body motion, in the plane of normalized amplitude and frequency. We find transitions in certain regions of this plane where the character of the fluid forces changes between distinct modes. Interestingly, these transitions correspond well with boundaries separating different vortex shedding modes in the Williamson-Roshko (1988) map of regimes. A further new characteristic, which is only observable with very high-resolution data, is the existence of regimes where two modes overlap. By examining the energy transfer from fluid motion to cylinder motion we are able to predict the response of an elastically mounted cylinder that agrees well with the measured free vibration response of Govardhan & Williamson (2006) at both high and low mass-damping. Furthermore, by looking at the shape of the excitation contours and the transitions between different modes, we are able to predict clearly the different types of transition between free vibration response branches; namely the hysteretic mode transition and the intermittent switching mode transition. A key approach that we shall introduce in this work involves the use of an "energy portrait", exhibiting stable and unstable amplitude response solutions, dependant on the gradient of energy transfer with amplitude (the sign of  $dE^*/dA^*$ ).*

### 1. INTRODUCTION

The problem of vortex-induced vibration is of interest to many fields of engineering. It affects, for example, the dynamics of riser tubes bringing oil from the seabed to the surface, the flow around heat exchanger tubes, and the design of civil engineering structures such as bridges and chimneys. An overview of recent phenomena in vortex-induced vibration can be found in the review by Williamson & Govardhan (2004).

The case of an elastically mounted rigid cylinder that is confined to move transversely to the flow is often used as a paradigm for understanding the problem of vortex-induced vibration in general. In many studies, investigators have employed controlled vibration (where a cylinder is moved with a prescribed motion) and related force measurements to the case of a freely vibrating cylinder. For example, Mercier (1973), Sarpkaya (1977), Staubli (1983) and Carberry et al. (2001, 2005) measured the forces on a cylinder that is controlled to oscillate sinusoidally transverse to a flow. Carberry et al. also used digital particle image velocimetry (DPIV) to examine the wake vortex dynamics. Gopalkrishnan (1993) and Hover, Techet & Triantafyllou (1998) made force measurements over a wide range of oscillation amplitudes and frequency, generating contour plots of the fluid forcing.

In the present study, we have conducted controlled vibration experiments over an expansive range of amplitude and frequency with much higher resolution than in any previous data set. Our hope is that with this extremely high resolution data, we may uncover key features that have not previously been observed, and thus obtain a more profound understanding of vortex-induced vibration.

Force measurements from controlled vibration experiments can be related to the free vibration case through the equation of motion. For an elastically mounted cylinder, constrained to move transverse to a flow, the motion ( $y$ ) can be defined by the following equation:

$$m\ddot{y} + c\dot{y} + ky = F(t) \quad (1)$$

When the body motion is synchronized with the vortex shedding, the cylinder motion,  $y(t)$  and fluid forcing,  $F(t)$  are typically well approximated by sinusoidal functions (in controlled vibration, the motion is prescribed to be sinusoidal):

$$y(t) = A \sin(2\pi ft) \quad (2)$$

$$F(t) = F_0 \sin(2\pi ft + \phi) \quad (3)$$

For such a system, the energy transferred from the fluid to the cylinder in one cycle is given by:

$$E_{IN} = \pi A F_0 \sin \phi \quad (4)$$

Where  $\phi$  is the important phase angle between body motion and fluid force. The energy lost to structural damping ( $c$ ) is given by:

$$E_{OUT} = 4\pi^3 c A f^2 \quad (5)$$

If the system is oscillating with a constant amplitude and frequency, the energy into the system must exactly balance the energy out of the system, over one cycle. Combining equations (4) and (5) and nondimensionalizing yields:

$$C_Y \sin \phi = \frac{4\pi^3 A^* (m^* + C_A) \zeta}{(U^* / f^*)^2 f^*} \quad (6)$$

(In this study  $A^* = A/D =$  amplitude/diameter,  $U^* = U/f_N D$ ,  $f^* = f/f_N$ , where  $U$  is the free stream velocity,  $f$  is the oscillation frequency, and  $f_N$  is the natural frequency, and  $m^* =$  oscillating mass / mass of fluid displaced.) We can use equation (6) for the energy balance along with contours of the fluid excitation ( $C_Y \sin \phi$ ) from controlled vibration to predict a free vibration response for any particular mass damping. By looking at the energy transfer in more detail, we can understand many of the phenomena that occur in free vibration, some of which we illustrate in this paper.

## 2. EXPERIMENTAL METHODS

The present experiments are conducted in the Cornell-ONR Water Channel, which has a cross-section of 38.1 cm x 50.8 cm. The turbulence level in the test section of the water channel is less than 0.9%. A cylinder of diameter 3.81 cm and length 38.1 cm is suspended vertically in the water channel and forced to oscillate transverse to the flow using a computer-controlled motor attached to a transverse lead screw. The flow speed (corrected for blockage) is 10.5 cm/s giving  $Re = 4,000$ . A fixed end plate is placed 2 mm below the bottom of the cylinder (but not in contact with the cylinder) to encourage two-dimensional vortex shedding, following the study of Khalak & Williamson (1996).

A total of 5680 runs are conducted over a range of normalized amplitude and frequency, for approximately 500 hours worth of data. Such an expansive data set is only possible because the experiment is conducted in a continuously flowing water channel facility and thus can be automated and run unattended for wide sets of data.

A two-axis force balance utilizing LVDTs (linear variable distance transducers) is used to measure the lift and drag forces on the cylinder. The transverse displacement of the cylinder is measured using a

non-contact (magnetostrictive) position transducer. The inertial forces in the transverse direction are subtracted from the total measured force.

For each run, the fluid force magnitude and phase angle (relative to the body motion) at the body oscillation frequency is calculated using a Fourier analysis.

## 3. CONTOURS OF FLUID EXCITATION AND VORTEX SHEDDING MODES

From this large amount of controlled vibration data, we can plot high resolution contours of several quantities:  $C_Y$ ,  $C_D$ ,  $\phi$ ,  $C_Y \sin \phi$ , etc. Here we choose to focus on the fluid force in phase with the cylinder velocity,  $C_Y \sin \phi$ , which represents the normalized fluid excitation.

Upon examining our controlled vibration data, we notice that the fluid forcing shows qualitative jumps in certain regions as amplitude or frequency is varied. We notice (in Figure 1) that the boundaries separating these different fluid forcing regimes are remarkably similar to boundaries separating different vortex wake modes in the Williamson & Roshko (1988) map of vortex shedding regimes. Thus we expect that the jumps in fluid forcing found here would correspond to changes in the wake vortex dynamics found in the latter work.

Using PIV measurements we have confirmed that the vortex shedding modes we expect to see, based on the Williamson-Roshko map, are indeed the shedding modes that exist for our oscillating cylinder. We show in Figure 2 two examples of such vortex wake modes: the “2S” mode and “2P” mode.

There are also some regions where even for a cylinder oscillating at a constant amplitude and frequency (i.e. at a particular point in the plot of Figure 1), the fluid forcing switches between two distinct modes. These two modes were analyzed separately and are shown as overlapping contours in Figure 1. This is particularly evident for the region between  $U^*/f^* \approx 4.4 - 6.2$ . Interestingly, the peak amplitude for a free vibration response exists inside this overlapping region, so our understanding of this region is essential to an understanding of the dynamics of the cylinder at its maximum (i.e. worst case) vibration.

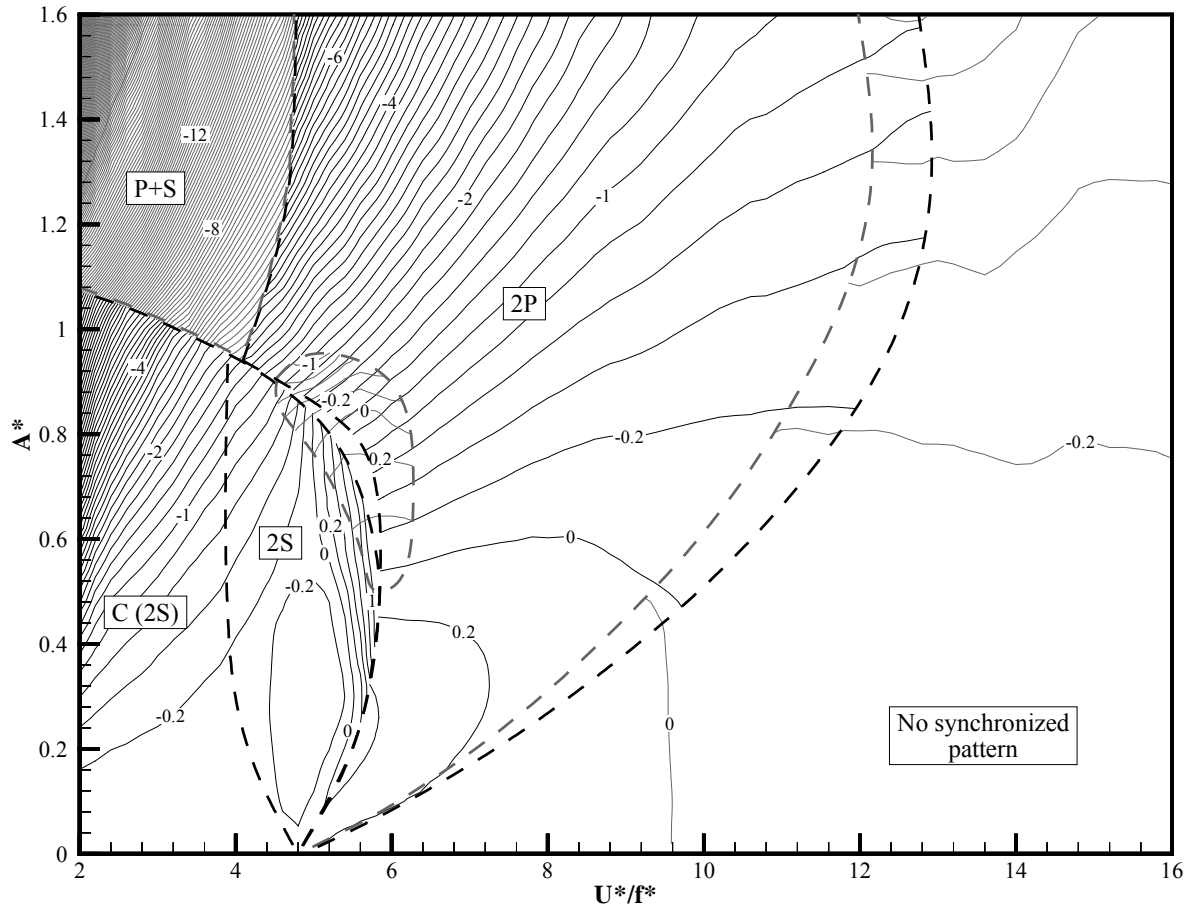


Figure 1. Extremely high resolution contours of fluid excitation ( $C_y \sin \phi$ ) in normalized amplitude-frequency plane. Boundaries between regimes of distinct fluid forcing (---) are remarkably similar to boundaries in the Williamson & Roshko (1988) map of wake modes. In regions where contours overlap, two modes can alternately exist for a given value of normalized amplitude and frequency.

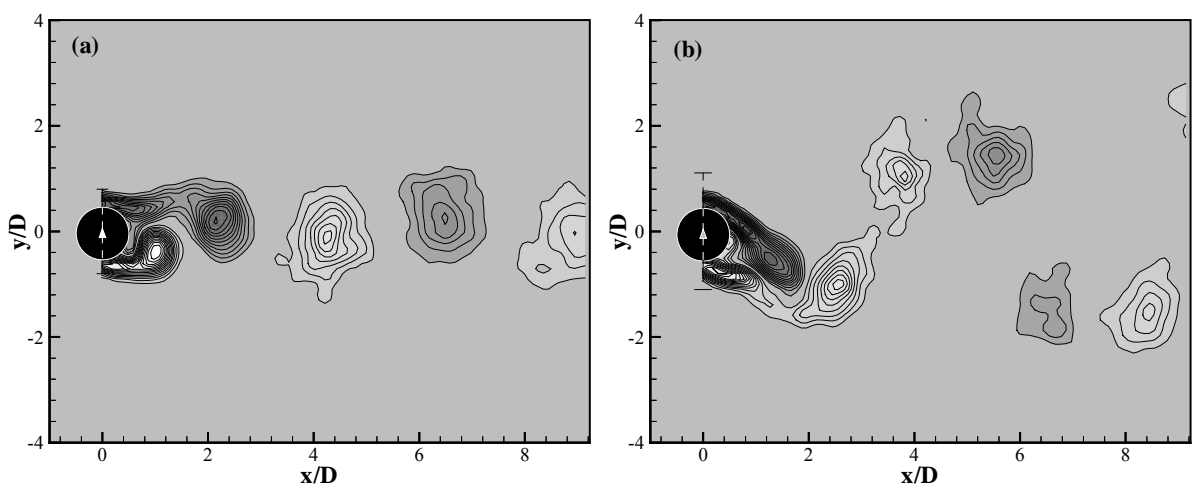


Figure 2. Vorticity contour plots from PIV measurements, illustrating the 2S and 2P vortex shedding modes. The 2S mode (a) was found at  $A^* = 0.3$ ,  $U^*/f^* = 5.4$ . The 2P mode (b) was found at  $A^* = 0.6$ ,  $U^*/f^* = 6.4$ . The darker gray indicates clockwise vorticity, the lighter gray indicates counterclockwise vorticity. Contour levels shown are  $wD/U = \pm 0.4, \pm 0.8, \pm 1.2, \dots$

#### 4. PREDICTING “FREE VIBRATION” RESPONSE

From the contour plot of the fluid excitation in Fig. 1, we can use equation (6) to predict the response for an elastically mounted cylinder and compare it to a measured free vibration response at the same mass-damping from Govardhan & Williamson (2006) as shown in Figure 3. There is a good agreement between the two cases, especially in the lower branch. The Reynolds numbers for the two cases are matched to be around 4000 for the peak amplitude. This is important, as the amplitude in the upper branch depends strongly on  $Re$  as explained in Govardhan & Williamson (2006). Similar agreement between the measured and predicted response is also found for higher values of mass-damping.

##### 4.1 Hysteretic mode transition: energy portrait at $U^* = 5.4$

For a free vibration response at low mass damping (such as the one shown in Figure 3) there are three branches: an initial, upper, and lower branch, with a hysteretic mode transition between the initial and upper branch, and an intermittent switching mode transition between the upper and lower branch (as shown by Khalak & Williamson, 1999). We can use the fluid excitation contours to help understand the origin of these transitions. For

example, for a cut of constant normalized velocity that intersects the initial and upper branch ( $U^* = 5.4$ ), the fluid excitation follows an ‘S’ like shape as amplitude is increased (see Figure 4). The energy lost due to damping follows a straight line with a slope proportional to the value of mass-damping. The free vibration response should lie at the intersections of these two curves where there is a balance of energy. In Figure 4, for a mass-damping of 0.05 there are three intersections, *however only two of them are stable*, having a negative gradient of energy transfer with amplitude ( $dE^*/dA^* < 0$ ). (We define  $E^*$  as the normalized energy transferred into the system over one cycle of oscillation.) These stable equilibria correspond to the initial branch and the upper branch of free vibration. The middle intersection is *unstable* ( $dE^*/dA^* > 0$ ). If the system were to be perturbed from this equilibrium at ‘U’, say the amplitude is increased slightly, the energy into the system would be greater than the energy out of the system and the amplitude would continue to increase until the system approaches the stable solution at ‘S’. In essence, stability and instability in the energy portrait is given by:

$$\begin{aligned} \text{Stable response solution:} & \quad dE^*/dA^* < 0 \\ \text{Unstable response solution:} & \quad dE^*/dA^* > 0 \end{aligned}$$

Steady free vibration would not be found at the unstable equilibria, so they would not appear in a

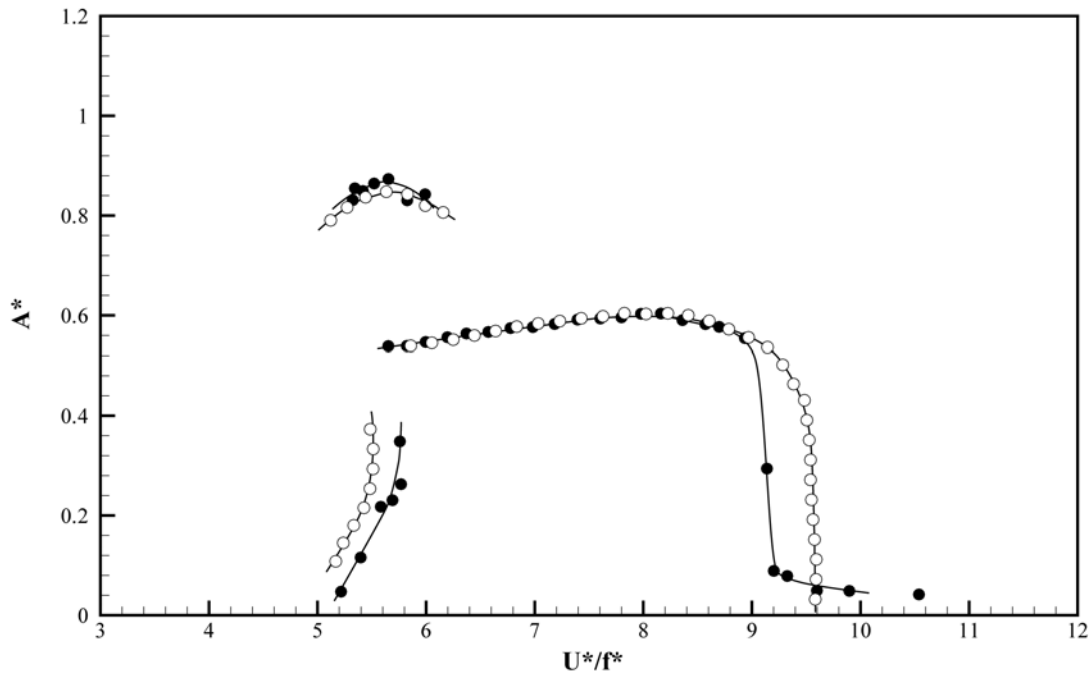


Figure 3. Close agreement is found between a measured free vibration response and predictions using high resolution controlled vibration force data;  $m^* = 10.47$ ,  $(m^* + C_A)\zeta = 0$ . ● measured response from Govardhan & Williamson (2006) ○ predicted response from controlled vibration data (present results). For the predicted response,  $Re = 4000$  throughout the plot. For the measured free vibration response, the peak amplitude corresponds to  $Re \approx 4000$ .

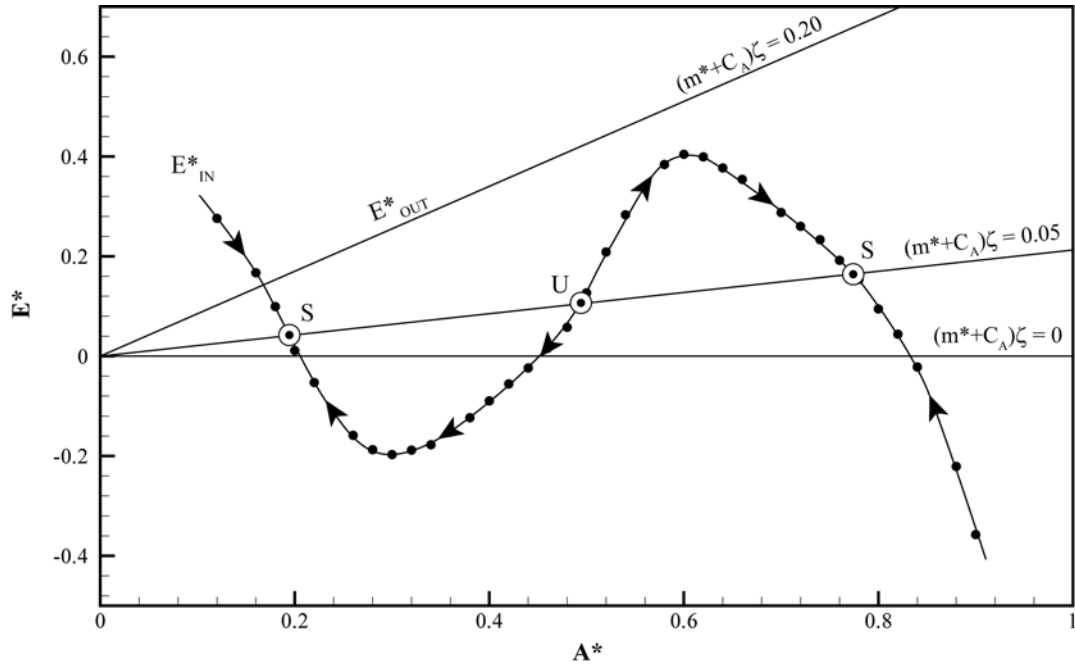


Figure 4. “Energy portrait” for the hysteretic mode transition ( $U^* = 5.4$  cut). ● fluid excitation from contours in Figure 1, ⊙ equilibrium points,  $S$  = stable equilibrium,  $U$  = unstable equilibrium. Arrows indicate direction of movement for non-equilibrium states.

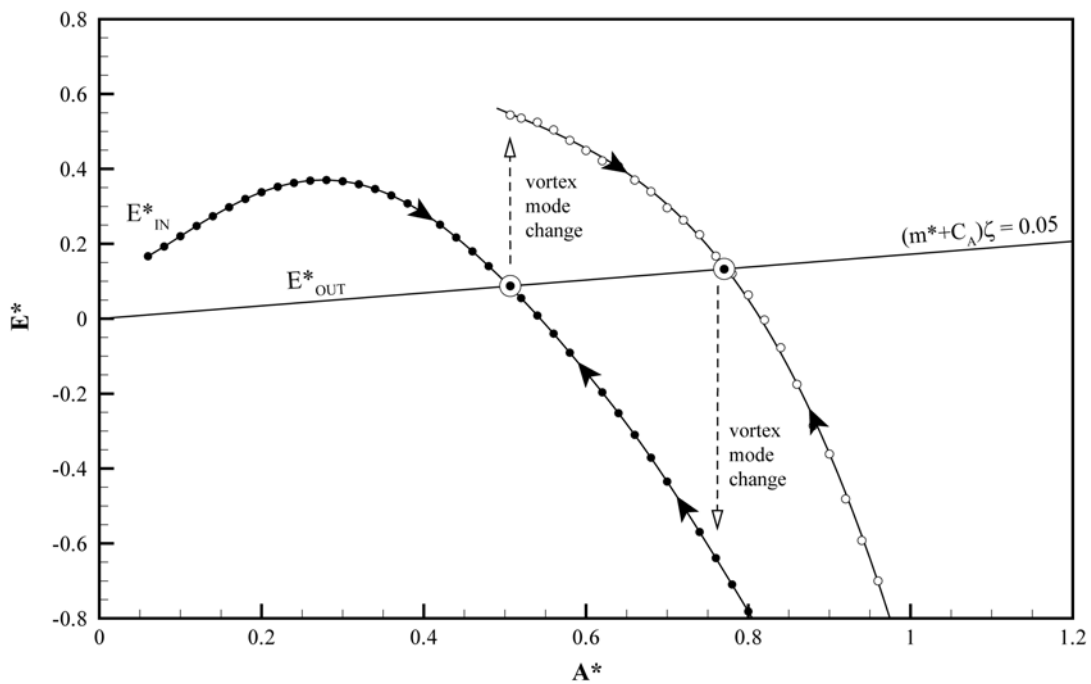


Figure 5. “Energy portrait” for the intermittent switching mode transition ( $U^* = 6.0$  cut). ●, ○ fluid excitation from the overlapping contours in Figure 1 (corresponding to the lower branch and the upper branch respectively). We suggest that an intermittent vortex mode change causes a jump from one fluid excitation curve to the other. ⊙ equilibrium points, arrows indicate direction of movement for non-equilibrium states.

response plot. The movement and disappearance of these stable and unstable equilibria, as normalized velocity is varied, is what leads to the hysteresis between the initial and upper branches that is seen in the response of elastically mounted cylinders.

#### 4.2 Intermittent switching mode transition: energy portrait at $U^* = 6.0$

We can also look at the fluid excitation along cuts of constant normalized velocity where the upper and lower branches are intersected,  $U^* = 6.0$ , passing through a large region where the fluid excitation contours overlap. In Figure 5, we see that there are amplitudes where two possible values exist for the fluid excitation. We find two stable equilibria, because for both cases where the energy of excitation is balanced by the energy dissipated by damping (in this example  $(m^* + C_A)\zeta = 0.05$ ) we note that  $dE^*/dA^* < 0$ . It seems plausible, based on previous free vibration results (i.e. Khalak & Williamson, 1999), to suggest that the vortex shedding may change intermittently between the two modes in the overlap region (see the contours in Figure 1). When this occurs, the system will jump from one fluid excitation curve to another, as illustrated by the paths followed in the “energy portrait” of Figure 5, leading to a distinct change in response amplitude. This scenario represents an intermittent switching of response modes, corresponding well with what is observed in free vibration.

### 5. CONCLUSIONS

The contours of fluid excitation shown here have been obtained from precise controlled vibration experiments with a much higher resolution than in any previously existing data sets. Here we have shown just a few examples of the type of analysis that can be performed with these contours. We have studied the energy balance along constant normalized velocity cuts through the fluid excitation contour plot within the amplitude-frequency plane. This allows us to gain a deeper understanding of the mode transitions that occur in free vibration. The hysteretic mode transition occurs because of the ‘S’ shape of the fluid excitation contours, leading to two possible stable amplitude response solutions at a given flow velocity, with an unstable solution found at an amplitude between the stable states, where  $dE^*/dA^* > 0$ . The intermittent switching mode transition, on the other hand, occurs because of the existence of overlapping vortex mode regimes.

We intend to present results and phenomena described here, as well as to discuss further controlled vibration results, transient behaviors, and

to examine the effects of mass ratio, damping, and Reynolds number

### 6. REFERENCES

- Carberry, J., Sheridan, J., & Rockwell, D. O. 2001. Forces and wake modes of an oscillating cylinder. *J. Fluids Struct.* **15**: 523-32.
- Carberry, J., Sheridan, J., & Rockwell, D. O. 2005. Controlled oscillations of a cylinder: forces and wake modes. *J. Fluid Mech.* **538**: 31-69.
- Gopalkrishnan, R. 1993. *Vortex-induced forces on oscillating bluff cylinders*. Ph.D. Thesis. MIT, Cambridge, MA.
- Govardhan, R. N. & Williamson, C. H. K. 2006. Defining the ‘modified Griffin plot’ in vortex-induced vibration: revealing the effect of Reynolds number using controlled damping. *J. Fluid Mech.* **561**: 147-180.
- Hover, F. S., Techet A. H. & Triantafyllou, M. S. 1998. Forces on oscillating uniform and tapered cylinders in crossflow. *J. Fluid Mech.* **363**: 97-114.
- Khalak, A. & Williamson, C. H. K. 1996. Dynamics of a hydroelastic cylinder with very low mass and damping. *J. Fluids Struct.* **10**: 455-472.
- Khalak, A. & Williamson, C. H. K. 1999. Motions, forces and mode transductions in vortex-induced vibrations at low mass-damping. *J. Fluids Struct.* **13**: 813-851.
- Mercier, J. A. 1973. *Large amplitude oscillations of a circular cylinder in a low speed stream*. Ph.D. Thesis. Stevens Inst. Tech., Hoboken.
- Sarpkaya, T. 1977. Transverse oscillations of a circular cylinder in uniform flow. *Rep. No. NPS-69SL77071, Nav. Postgrad. Sch., Monterey, CA.*
- Staubli, T. 1983. Calculation of the vibration of an elastically mounted cylinder using experimental data from forced vibration. *ASME J. Fluids Eng.* **105**: 225-29.
- Williamson, C. H. K. & Roshko, A. 1988. Vortex formation in the wake of an oscillating cylinder. *J. Fluids Struct.* **2**: 355-381.
- Williamson, C.H.K. & Govardhan, R. 2004. Vortex-induced vibrations. *Ann. Rev. Fluid Mech.* **36**: 413-455.